Cancer Letters 442 (2019) 53–67

Contents lists available at ScienceDirect

Cancer Letters

journal homepage: www.elsevier.com/locate/canlet

Original Articles

Genomic sequencing and editing revealed the GRM8 signaling pathway as potential therapeutic targets of squamous cell lung cancer

Panpan Zhang[a,1], Bin Kang[b,c,d,1], Guoyun Xie[b,c,1], Shaolei Li[a,1], Ying Gu[b,c,d,1], Yue Shen[b,c,d,1], Xin Zhao[b,c,1], Yuanyuan Ma[a], Fuqiang Li[b,c], Jiahui Si[a], Jian Wang[b,c], Jinfeng Chen[a], Huanming Yang[b,c,d], Xun Xu[b,c,d,*], Yue Yang[a,**]

[a] Department of Thoracic Surgery II, Key Laboratory of Carcinogenesis and Translational Research, Ministry of Education/Beijing, Peking University Cancer Hospital and Institute, Beijing, China
[b] BGI-Shenzhen, Beishan Industrial Zone, Shenzhen, 518083, China
[c] China National GeneBank, BGI-Shenzhen, Jinsha Road, Shenzhen, 518120, China
[d] Guangdong Provincial Key Laboratory of Genome Read and Write, Jinsha Road, Shenzhen, 518120, China

ARTICLE INFO

Keywords:
Sequencing
Genome editing
GRM8
Lung cancer
Therapeutic targets

ABSTRACT

The study sought to explore novel genetic aberration driving squamous cell lung carcinoma (LUSC). The whole exome (WES), whole genome (WGS) and target region (TS) sequencings and CRISPR-Cas9 genome editing techniques were integrated to explore and validate novel targeting candidates from LUSC primary tumors and corresponding patient-derived xenografts (PDXs). Seven genes (*FGFR2, GRM1,PIK3CG*, *PIK3CA,ZFHX4*, *CSMD3*, *GRM8)* with high frequencies of both single nucleotide variants (SNVs) and copy number variants (CNVs), and two genes (*CLDN1* and *RIT1)* only with CNVs were identified by bioinformatics analysis. The functions of these candidates were validated through CRISPR-Cas9 system in primary PDX cells. Furthermore, we focused on the genetic and functional analysis of Metabotropic glutamate receptor 8 (GRM8), whose transcriptional activation was elucidated to promote the survival of LUSC tumor cell through inhibiting cAMP pathway and activating MAPK pathway. The SNV identified in GRM8, A112G, activated downstream signaling pathway and induced cell proliferation, which could be reversed by cAMP stimulator and MEK inhibitor. In conclusion, the components of GRM8 signaling pathway could serve as potential targets of squamous cell lung cancer carrying GRM8 activating variants.

1. Introduction

Lung cancer is the leading cause of cancer death worldwide [1]. Squamous cell carcinoma (LUSC) ranking at the second of total lung cancer incidence [2]. Targeted therapies against some frequently mutated genes, such as *EGFR*, *ALK*, *MET* have proven to bring better clinical outcomes to adenocarcinoma patients carrying corresponding mutations. In contrast, little is known for LUSC [3]. Lack of mutation hotspot and functional validation of mutation might be responsible for the few driver gene identified in LUSC. Therefore, efforts towards the identification and validation of driver mutations of LUSC are still needed, which are essential for the future development of targeted therapies.

Accumulating evidence demonstrates that high consistency of drug activities and response rates between PDXs and patients, supporting PDX as a robust preclinical model for validating the cancer targets and evaluating the utility and efficacy of anticancer drugs [4]. Although many studies have applied CRISPR (Clustered Regularly Interspaced Short Palindromic Repeats) system to screen gene targets involved in the tumor initiation, progression, metastasis and therapeutic resistance in various cancer cell-lines [5,6], there is still very limited study in primary PDX tumor cell, which might provide more clinically relevant

Abbreviations: LUSC, lung squamous cell lung carcinoma; PDX, patient derived xenograft; GRM8, metabotropic glutamate receptor; WES, whole exome sequencing; WGS, whole genome sequencing; TS, target region sequencing; CRISPR, Clustered Regularly Interspaced Short Palindromic Repeats; NT, Non-targeting control; EV, empty vector control

* Corresponding author. BGI-Shenzhen, Beishan Industrial Zone, Shenzhen, 518083, China.
** Corresponding author.
E-mail addresses: xuxun@genomics.cn (X. Xu), zlyangyue@bjmu.edu.cn (Y. Yang).
[1] Equal contribution.

https://doi.org/10.1016/j.canlet.2018.10.035
Received 6 June 2018; Received in revised form 18 October 2018; Accepted 24 October 2018

result.

Therefore, we integrated genomic sequencing technique, CRISPR/Cas9 system and PDX models to identify and validate the potential driver gene targets. In our study, we first selected 11 groups of high-quality LUSC PDX tumor and matched primary tumor tissue samples for WES and WGS analysis. Through predicting the driver functions of mutated genes using iCAGES tool [7], and analyzing the mutation frequencies both in our samples and LUSC cohorts of The Cancer Genome Atlas (TCGA) [8], more than 300 significant genes carrying SNVs were identified from WES data. And through searching COSMIC database [9] and previous publications, 143 significant genes carrying CNVs in at least two cases were identified from WGS data. Then 56 genes carrying highly frequent SNVs or CNVs were verified through target region captured sequencing (TS) in the LUSC samples for WES and WGS sequencing, and in additional 70 pairs of matched primary tumor and control normal samples. The functions of 9 significant candidates with relatively high mutation frequencies were assessed in the primary PDX cells through CRISPR-Cas9 loss-of-function system. Furthermore, we focused on a novel candidate, GRM8, to investigate its tumor-promoting functions and its activating mutations identified in LUSC tumor samples. Our study thus provides an integrated approach to identify and characterize novel driver genes that have been implicated in LUSC.

2. Materials and methods

2.1. Establishment of PDX mouse models from the surgically resected LUSC tissues

Fresh surgical specimens were cut to about 2 mm^3 in size and implanted into the flank subcutaneous space of non-obese severe combined immune deficient (NOD-SCID) mice (2 or 3 mice/patient specimen). The time course from the inoculation of surgical specimen until the harvest of first generation of patient-derived xenograft (PDX) (1.5 cm in diameter) ranged from 2 to 6 months, with an average of 3 months. Once the tumors reached 1–1.5 cm in diameter as measured with calipers, the mice were euthanized and tumors were passaged serially into new NOD-SCID mice for at least three times to establish stable models. The tumors (labeled as P1 for the first passage in animals) were divided into 2–3 mm^3 specimens, and were frozen in liquid nitrogen for future investigation or implantation to generate more xenografts (P2, P3, etc.). The animal care was in accordance with institution guidelines.

70 paired frozen tumor tissues from the lung squamous patients who underwent radical surgery at Peking University Cancer Hospital & Institute were used for target sequencing in this study. This study was approved by the Ethics Committee of Peking University Cancer Hospital (No. 2015KT71), and all participants provided the informed consents to participate in this research.

2.2. HE staining

Formalin-fixed and paraffin-embedded primary LUSC and PDX tumor samples were cut into sections and stained with hematoxylin and eosin (H&E). Histopathology was reviewed by an experienced pathologist.

2.3. Genomic DNA preparation

The genomic DNA from tissues was prepared using the QIAamp DNA Mini Kit (Qiagen) following the manufacturer's instructions. The quantity and quality of DNA were determined by agarose gel electrophoresis or Agilent 2100 analyzer. Mass spectrometric fingerprint genotyping of 21 common SNPs was performed for all the samples before sequencing to verify that matched primary tumor, control normal, and P1 and P3 xenograft tumor tissues were derived from the same patient.

2.4. Whole exome sequencing

Prior to the library construction, 2–3 μg of genomic DNA from each sample was fragmented using a Covarias sonication system to mean sizes of B500bp. After fragmentation, libraries were constructed according to the Illumina Paired-End protocol. Briefly, the purified, randomly fragmented DNA was treated with a mix of T4 DNA polymerase, Klenow fragments, T4 polynucleotide kinase and a nucleotide triphosphate mix to repair the ends by blunting and phosphorylation. The blunted DNA fragments were subsequently 3'-adenylated using the Klenow fragment (3'–5'exo) and ligated by T4 DNA ligase to BGI-designed PE Index Adaptors that had been synthesized with 5'-methylcytosine in place of cytosine. After each step, the DNA was purified using the QIAquick PCR Purification Kit (Qiagen). 3 mg genomic DNA from each sample was fragmented and ligated PE Index Adaptors, then captured with Nimblegen Human EZ V3 64 Mb Kit as described in the protocol for the Target Enrichment System for an Illumina Paired-End Sequencing Library.

All the constructed libraries were sequenced on HiSeq X10 platform using two 100-bp paired-end reads. The sequencing reads containing adaptor sequence and low-quality reads, which have too many Ns ($> 10\%$) and low-quality base ($> 50\%$ bases with quality < 5) were removed before sequence alignment.

2.5. Whole genome sequencing

The library construction and sequencing were carried out as described in previous report [10]. Briefly, the genomic DNA was fragmented by ultrasound on Covaris E220 (Covaris) to DNA fragments between 50bp ~ 800bp according to the manufacturer's instructions. The fragmented DNA was further selected to 100bp ~ 300bp by AMPure XP beads (AGENCOURT). The selected DNA fragments were then repaired to obtain a blunt end and modified at 3‘end to get a dATP as a sticky end. The dTTP tailed adapter sequence was ligated to both ends of the DNA fragments. The ligation product was then amplified for 8cycles and subjected to the following single strand circularization process. The PCR product was heat-denatured together with a special molecule which was reverse complemented to one special strand of the PCR product, and the single strand molecule was ligated using DNA ligase. The remaining linear molecule was digested with the exonuclease, finally obtaining a single strand circular DNA library.

The whole genome sequencing was conducted on the BGISEQ-500 platform using 50bp paired-end reads. There were three steps including making DNBs, loading DNBs and sequencing. For making DNBs, a 6 ng single strand circular DNA library was first PCR amplified for 10 min in an 80 μl reaction volume with pure water, buffer and DNB polymerase. After PCR reaction, 20 μl DNBs stopping buffer was added to terminate the PCR reaction. Finally, we used the Qubit® ssDNA Assay Kit to quantify the DNBs on a Qubit® Fluorometer (concentration ≥ 10 ng/μl). For loading DNBs, we first added 33 μl DNBs loading buffer to DNBs product from the last step, and the mixture was placed on the BGIDL-50 (the sample preparation machine). Then we selected the DNBs loading process (Version: sample load 2.0) to load DNB onto the sequencing chip, which included 96 min' loading time and 30 min’ incubation at room temperature. Finally, for sequencing, we followed to the BGISEQ-500 protocol. We selected sequence control software Version 1.1.0.10003, sequence process Version 1.0.06 and Zebracall process Version 0.5.0.13875 for sequencing. Sequencing was initiated after the sequencing reagents pre-loaded and sequencing chip installed, and this process was finished in ~72 h.

2.6. Validation of somatic mutations

Target region captured sequencing (TS) on a set of 56 selected genes

was used to validate the status of identified SNVs and CNVs. One microgram of genomic DNA from each sample for validation was used for hybrid capture and library construction. Libraries were then sequenced on BGI-Seq500 platform using 100bp paired-end reads sequencing.

2.7. Data analysis and mutation analysis

Paired-ended reads of WES and WGS were filtered by SOAPnuke [11](N rate > 10%, low quality rate > 50% with quality < 5) and mapped to the UCSC human reference genome(hg19) by BWA [12]. The WES and TS data were aligned using BWA-MEM(bwakit-0.7.15). The WGS data were using BWA-BACKTRACK(bwa-0.6.2). Filtered reads of PDX were additionally mapped to the UCSC mouse reference genome (mm10) by BWA-MEM. The identification of human-specific and common mouse-graft reads were performed respectively based on collecting and comparing the read ids of the human/mouse aliments. Due to human-mouse reads mapped against the human genome and mouse genome with different score, the common host-graft reads with lower quality mapped to mouse were discarded by XenofilteR. Alignments were then sorted by Picard [13](WES, v2.7.1) or Sambamba [14](WGS, v 0.6.3), marked duplicates by Clinsek [15](WES, v0.1) or Picard(WGS, v2.7.1),and base recalibration were performed using GATK [16](v3.4). After fundamental analysis, somatic SNVs and INDELs were identified by multiple tools using WES data. 1) Somatic SNVs and INDELs of a tumor sample (T/P1/P3) were identified data against with the corresponding normal sample by GATK Indelocator(v2.3-9) (default parameters, and mutations labeled SOMATIC were retained), MuSE [17](v1.0rc) (default parameters, and mutations labeled PASS and SOMATIC were retained), MuTect2(as part of the GATK)(-retry 3 -tbc 300 -maxConcurrentRun 200, -sc 100, otherwise default parameters, and mutations labeled PASS were retained), Platypus [18](v 0.8.1)(–filterDuplicates = 1 –nCPU = 4, otherwise default parameters, and mutations labeled PASS were retained), SomaticSniper [19](v1.0.5.0) (default parameters, and mutations with SSQ ≥ 25 were retained) and VarScan2 [20](v2.4.3) (default parameters, and mutations with SSQ ≥ 25 and labeled with PASS were retained) respectively. Somatic SNVs and INDELs detected by at least two tools were retained. 2) Somatic SNVs and INDELs of multiple related tumor samples were identified by multisnv [21](default parameters) and Platypus(v 0.8.1)(–filterDuplicates = 1 –nCPU = 4,and otherwise default parameters) respectively. Somatic SNVs and INDELs detected by both two tools were retained. In TS data, somatic SNVs and INDELs of a tumor sample (T/P3) were identified against the corresponding normal sample by MuTect and Platypus.

Somatic Copy number variations (CNVs) and Structure variations (SVs) were called by FACETS [22](v0.5.6)(-Q 20 -r 10,0,otherwise default parameters) and Novobreak [23](v1.1.3, default parameters) using WGS data, respectively.

2.8. Elimination of mouse-derived reads

First, the adopted strategy was to align all reads to the human genome(hg19) and mouse genome(mm10) by BWA. Second, the identification of human-specific and common mouse-graft reads were performed respectively based on collecting and comparing the read IDs of the human/mouse aliments. Third, due to human-mouse reads mapped against the human genome and mouse genome with different score, the common host-graft reads with higher quality mapped to human were retained. After discarding, the estimated proportion of mouse-specific reads ranged from about 7.48% to 13.57% approximately, depending on different PDX samples.

2.9. Mutation allele frequency (MAF) analysis

The MAF was defined as the reads carry the alteration allele divided by total reads covering the single nucleotide positions. We used Bamreadcount [24] to generate the metrics of all somatic mutations from the primary tumor and PDX tumor BAM files in each patient and regarded the depth and count of alteration base as total reads and mutated reads number respectively. Furthermore, the MAF of each sample was corrected based on the tumor purity through PyClone software [25].

2.10. Prediction of driver genes and KEGG enrichment analysis

In each patient, based on the overlapping somatic mutations in T/P1/P3, driver gene candidates were predicted by the iCAGES tool with the default parameters. We regarded the genes labeled with driver by iCAGES as driver genes. All driver genes of 11 patients were implemented to KEGG pathway enrichment analysis by GSEA [26]. KEGG pathways with q-value < 0.01 and genes in overlap > 5 were considered to be significantly enriched for driver genes. Then, owing to characterize the functional of the driver genes, cancer-related pathways were removed.

2.11. Vector construction

The loss-of-function lentiviral vector, Lenti-CMV::SaCas9-2A-GFP;U6::BsaI-sgRNA was constructed by the Gateway recombination reaction between the donor vector containing synthetic SaCas9-2A-GFP and sgRNA expressing elements flanked by attL sequences and the destination vector containing attR sequences, pLEX_305 (#41390, Addgene). The sgRNAs were designed using the Benchling tool (https://benchling.com), and the most efficient sgRNA was chosen and inserted into the BsaI sites after annealing. The CRISPRa vectors of SAM system include lenti- dCAS9-VP64_Blast (#61425, Addgene), lenti MS2-P65-HSF1_Hygro (#61426, Addgene), and lenti sgRNA(MS2) zeo backbone (#61427, Addgene). The sgRNAs were also designed using Benchling tool and were inserted into the BsmBI sites after annealing. The vector to construct SNVs in 293T cells was pSpCas9(BB)-2A-Puro (PX459) V2.0 (#62988, Addgene). The sgRNAs were also designed using Benchling tool, and were inserted into the BbsI sites after annealing. The 127bp oligos used as the templates of SNV construction were synthesized in IDT. The plasmid over-expressing wild-type GRM8, pENTER-GRM8 was constructed by cloning the coding sequence (CDS) of GRM8 into pENTER plasmid using restriction sites of *AsisI* and *MluI*. The plasmid over-expressing mutant GRM8 (A112G) was constructed by replacing a DNA fragment of wild-type GRM8 with the synthesized fragment containing corresponding mutation through restriction sites of *AsisI* and *EcoRI*.

2.12. T7E1 assay

The sgRNA efficiencies were tested in 293T cells through T7E1 assay. The 293T cells were transfected with the loss-of-function lentiviral vectors carrying sgRNAs using Lipofectamine3000 reagents (Thermofisher Scientific). After 48 h, genomic DNA was extracted, and the DNA fragment containing breakpoint was PCR amplified. The PCR product was digested by T7 endonuclease I (NEB) after annealing and was presented by agarose gel electrophoresis.

2.13. Packaging lentivirus

The lentiviral vector and packaging plasmids VSVG and psPAX2 (#8454 and #12260, Addgene) were co-transfected into HEK293T cells through calcium phosphate precipitation. The lentivirus was pelleted by centrifuging the culture medium at 25000 rpm and 4°C for 2 h, and was resuspended using 1640 medium and stored in −80 °C.

2.14. Culture and infection of PDX tumor cells

The PDX tissue was cut into 2–3 mm pieces and washed for 3 times

with PBS. The tissue was digested by collagenase II and IV for 1–2 h and filtered through a sterile nylon cell strainer (FALCON). The cells were cultured in 1640 medium with 10% FBS for 1 week in the plate with low attachment surface (CORNING) and stored in liquid nitrogen. Before virus infection, the PDX cells were thawed and cultured for 24 h. Fifty thousand cells were seeded into 96-well plate with low attachment surface (CORNING) and were transduced with concentrated lentivirus and 8 ng/ml Polybrene for 48 h before collected for viability assay.

2.15. Culture and treatment of cell-lines

Human LUSC cell-line EBC-1 and SKMES-1 cells were respectively cultured in MEM and 1640 medium, supplemented with 10% fetal bovine serum (FBS), 1% Nonessential Amino Acids (NEAA), 1 mM Sodium Pyruvate (NaP) (Thermofisher Scientific), and 293T cell was cultured in DMEM medium plus 10% FBS. All of them were cultured in a humidified atmosphere of 5% CO2 at 37 °C incubator. The cAMP activator Forskolin and MEK1 inhibitor Selumetinib (Selleck Chemicals) were dissolved in DMSO and the treating concentrations mentioned in Results.

2.16. Cell viability, cell proliferation and cytotoxicity assays

The viability of PDX cells infected with lentivirus or treated with reagents was detected using CellTiter-Glo® 2.0 kit (Promega) according to the kit instruction. Briefly, fifty thousand cells were seeded in 96-well plate and treated with specific reagents or infected with virus. After treatment, the cells were collected by centrifugation. One hundred microliter CellTiter reagent was added, and the mixture was incubated at room temperature and under darkness for 10 min. Then the luminescence was recorded. Three replicates were conducted. The proliferation of cell-lines transfected with CRISPRa system or treated with reagents were assessed using cell counting or CCK-8 Kit (DOJINDO Laboratories) according to the kit instruction. Briefly, five thousand cells were seeded in 96-well plate and cultured overnight. After treatment, 10 μl CCK-8 reagent was added and incubated at 37 °C for 2 h. The absorbance was measured at 450 nm using a spectrophotometer. Three replicates were conducted. The cytotoxicity assay was conducted using the lactate dehydrogenase (LDH) release kit (DOJINDO Laboratories) according to the kit instruction.

2.17. Reverse transcription and quantitative real-time PCR (qPCR)

RNA was extracted using Trizol (Invitrogen, Carlsbad, CA, USA) according to the manufacturer's protocol. 2 μg of total RNA was transcribed with TransScript First-Strand cDNA Synthesis SuperMix (Cat No. AE301-02, Transgene biotech, Beijing, China). Subsequently, PCR was performed with GoTaq qPCR Master Mix (Cat No. A6001, Promega Corporation, Madison, USA). Cycling conditions were as follows: 5 min at 95 °C followed by 45 cycles each consisting of 10 s at 95 °C, 20 s at 60 °C and 30 s at 72 °C. The relative concentration of genes was normalized to β-actin. Fold change was calculated by the 2-△Ct method.

2.18. Western blot analysis

Proteins were extracted from cells using RIPA buffer containing complete protease inhibitor cocktail (Roche). Proteins were separated by SDS-PAGE gel and transferred to NC membranes. Membranes were blocked with 5% non-fat milk or 5% BSA followed by incubating with the primary antibodies against the following antigens: GRM8 (1:500 dilution, Absin Bioscience Inc), phospho-MEK, MEK, phospho-ERK, ERK, GAPDH (1:1000 dilution; Cell Signaling Technology). Signals were visualized using chemiluminescence instrument (Millipore). The blots were quantified and normalized by Image J software.

2.19. Measurement of intracellular cAMP level

Two thousand cells of interest were collected and lysed with 100 μl lysis buffer. Then the intracellular cAMP level was measured with an ELISA assay kit (Cell Signaling Technology) according to the manufacturer's protocol.

2.20. PKA activity assay

5×10^6-1×10^7 cells were collected and resuspended in 0.5 ml of cold PKA extraction buffer. After centrifuging for 5 min at 4 °C and 14000g, the PKA activity in the supernatant was measured with the substrate in the PepTag Assay Kit (Promega) according to the manufacturer's protocol.

2.21. Statistical analysis

All statistical analyses were performed using SPSS 20.0 software and GraphPad 6.0. The data were presented as the mean ± standard deviation (SD). A student's t-test or one-way ANOVA was used to assess differences of two or more groups of western blot results. Differences in cell proliferation and cell viability were conducted with two-way ANOVA. And the statistical significance was presented as followed: * $0.01 < P < 0.05$, ** $0.001 < P < 0.01$, ***$P < 0.001$.

3. Results

3.1. Sample description and sequencing statistics

To explore and validate novel therapeutic targets of LUSC, we selected 11 cases with high-quality PDX models for WES and WGS analysis. Among them, 8 cases had matched primary tumors (T), control normal samples (N) and passage 1 and 3 of PDX tumor samples (P1 and P3), while the rest missing passage 1 of PDX tumor samples. The clinical information of the 11 cases was shown in Table 1. Only one female case without smoking history was selected. Four patients had been treated with neoadjuvant chemotherapy prior to surgery, while 5 patients had developed the lymph node metastasis. The HE staining results of the tumor tissues for sequencing were shown in Supplemental Fig. 1. The high histological similarity was observed among the primary tumors and their corresponding PDX tumors, demonstrating that PDX models well retained the pathological features of their primary tumors.

The WES analysis was performed on 41 tissue samples of 11 LUSC cases using HiSeq X10 platform (Illumina), and reached the median fold coverage of 174 × (range 110-363 ×). For the PDX tumor samples, the XenofilteR (Roel Kluin, Oscar Krijgsman et al. unpublished observations) algorithm was used to separate the sequence reads derived from the xenograft and mouse and deplete the contaminated mouse reads. While the WGS analysis was performed on the primary tumor and control normal samples of the 10 cases with high rates of overlapping

Table 1
The clinical features of squamous cell lung cancer cases for sequencing.

ID	Gender	Age	Smoking	Stage	Treatment prior to surgery*
LUSC-006	M	70	Yes	IIIA(T2aN2M)	Yes
LUSC-012	M	53	Yes	IB (T2aN0M0)	No
LUSC-013	F	54	No	IA (T1bN0M0)	No
LUSC-015	M	64	Yes	IIA(T2aN1M0)	Yes
LUSC-016	M	73	Yes	IB (T2bN0M0)	No
LUSC-017	M	64	Yes	IIA(T2bN0M0)	No
LUSC-018	M	61	Yes	IIA(T2aN1M0)	Yes
LUSC-019	M	70	Yes	IB (T2bN0M0)	No
LUSC-020	M	65	Yes	IIA (T2N0M0)	No
LUSC-021	M	62	Yes	IIA(T2aN1M0)	Yes
LUSC-022	M	65	Yes	IIIA(T1bN2M)	No

mutations among T and P samples according to WES analysis, using BGISEQ-500 platform (BGI). The median fold coverage reached 68.14 × (range 55.73-72.1 ×).

To verify the mutations detected by WES and WGS, a target region captured sequencing was performed on a set of 56 selected genes with a median fold coverage of 1130 × (range 480-1863 ×) on custom target regions in the primary (T) and PDX (P3) tumor and control normal samples of 10 LUSC cases for WES and WGS analysis described above, and in the primary tumor and control normal samples of additional 70 LUSC cases.

3.2. Homology and heterogeneity of genomic alterations among primary and PDX tumors

According to WES analysis, the total somatic mutation numbers in primary (T) and PDX tumor (P1 and P3) samples of each case ranged from 235 to 2697, from 260 to 2707, and from 250 to 6151 respectively (Supplemental Table 1). To explore the homology of somatic mutations among T and P samples, the overlapping mutation number between T and P1 (O1) or between T and P3 (O3) was calculated and compared with the total mutation number of T sample (O1/T or O3/T). The values of O1/T and O3/T respectively ranged from 0.91 to 0.99 and from 0.71 to 0.98 (Fig. 1A, Supplemental Table 1). These high ratios demonstrated that the majority of somatic mutation in primary tumor retained in PDX tumors.

Furthermore, five mutation signatures were extracted from the somatic mutations of T and P samples according to different patterns of base substitutions through a published Bayesian NMF algorithm [27,28]. And the counts and proportions of these five signatures both remained consistent among most of the primary tumor and corresponding PDX tumor samples (Fig. 1B, upper and lower panels). Among the five mutation signatures, the signature related to smoking (W3) was the main signature, which corresponded to the COSMIC_Signature.4, and was observed in most of the tumor samples for WES analysis (Fig. 1B and Supplemental Table 2). As an exception, only P3 tumor sample of LUSC-018 had much more redundant mutations than its primary tumor sample. And majority of these redundant mutations were classified into W1 signature corresponding to COSMIC Signature 5, whose aetiology is unknown (Fig. 1B and Supplemental Table 2), which might result from the random mutagenesis occurring in the passage of PDX mouse model.

Moreover, four types of non-synonymous somatic mutations were identified from tumor samples: non-synonymous and nonsense SNVs, splicing mutation and Indel. The total numbers of non-synonymous somatic mutations in T, P1 and P3 samples of each case respectively ranged from 51 to 592, from 44 to 592, and from 44 to 585. And the proportions of these four mutation types of these three tumor samples were similar (Fig. 1C). A complete list of non-synonymous mutations of all the tumor samples was provided in Supplemental Table 3. All these non-synonymous mutations were also searched in TCGA database, and 28 recurrent mutations were listed in Supplemental Table 4. All the results shown here indicated that the LUSC PDX models established in our study faithfully reflected the molecular features of corresponding primary tumors.

Furthermore, similar as previous reports, the purities identified by FACETS analysis in the primary tumors (T) are lower than those in the PDX tumor samples (P1 and P3) (Supplemental Table 5), probably attributed to the relative enrichment of tumor cells in PDX samples. And the mutant allele frequencies (MAFs) of non-synonymous mutations identified by WES analysis with or without correction for tumor purities were presented in Fig. 1D and Supplemental Fig. 2 respectively. The MAFs without tumor purity correction in P1 and P3 tumors were significantly higher than those in primary tumors (Supplemental Fig. 2). In detail, the average MAFs without purity correction in primary, P1 and P3 tumors were respectively 0.398 (range 0.032–1.00), 0.595 (range 0.068–1.00), and 0.591 (range 0.099–1.00). And after purity correction, the average MAFs of primary, P1 and P3 tumors were respectively 0.97 (range 0.222–0.997), 0.976 (range 0.343–1) and 0.974 (range 0.269–1). The MAFs of different tumor samples after corrections were almost similar.(Fig. 1D). Only the mutations detected in the primary and PDX tumor samples of LUSC-017 case showed lower MAFs compared with other tumor samples. The results suggested that majority of the mutations detected our LUSC tumor samples were clonal events, and there were possibly more subclonal events in the mutations detected in LUSC-017 case compared with those in other cases.

3.3. Significant genes and pathways with SNVs identified by WES analysis

Aiming to identify novel targeting candidates, the iCAGES bioinformatic tool [7] was utilized to screen the potential driver genes in the overlapping SNV mutants of T, P1 and P3 samples identified by WES. Two hundred and ninety nine potential driver genes were identified, and the median number of driver events per sample was 30, ranging from 7 to 84. Their mutation frequencies and ranks both in our sequencing cohort and in the LUSC cohorts of TCGA database [29] were shown in Supplemental Table 6. In addition to these potential driver genes, forty two genes with over 20% SNV frequencies shared by T, P1 and P3 samples were also identified in order to broaden the candidate selection range. Most of those 42 genes had high mutation frequencies both in our cohorts and in LUSC cohorts of TCGA database (Supplemental Table 7). Twelve genes were both identified by the driver and frequency analysis, including *TP53*, *COL11A1*, *NOTCH1*, *RYR2*, *KMT2C*, *GRM1*, *TBXT*, *PIK3CG*, *BRCA2*, *EBF1*, *NOXA1 and MYH2*.

Many mutated genes were involved in the signaling pathways responsible for the initiation or progression of malignancy. The genes identified by the driver and frequency analysis were combined for KEGG pathway and were clustered into a batch of critical cancer-related pathways. The significant pathways containing the highest numbers of mutated genes included MAPK signaling (25), Focal adhesion (23), calcium signaling (19) and neuroactive ligand receptor interaction (19) pathways (Supplemental Fig. 3).

3.4. Significant genes with CNVs and fusion variations identified by WGS analysis

In order to identify the driver genes with structural variations, the primary tumor and control normal samples of 10 LUSC cases, except for LUSC-016, were analyzed by WGS sequencing, which had overlapping mutation rates higher than 80% among T, P1 and P3 samples according to WES analysis. The WGS analysis totally identified around 16000 CNVs, and 34 fusion variations with at least one breakpoint in the gene region (Supplemental Table 8). And these CNVs and structural variations were at least detected in two cases. The Circos plots demonstrated the overall status of structural variations in these 10 tumor samples (Supplemental Fig. 4). Through searching COSMIC database [9] and previous publications, 172 cancer-related CNV genes were screened out. One hundred and forty three of those CNV driver genes were detected in our WGS data. The copy numbers (CN) of these genes ranged from 0.45 to 11.10. These 143 driver genes carrying CNVs were listed in Supplemental Table 9 with their frequencies and ranks in our sequencing cohort and in the LUSC cohorts of TCGA database.

For the fusion genes identified by WGS analysis, we found the 5′ fragment of tumor suppressor gene, SET Domain Containing 3 (*SETD3*), on chromosome 14 was fused to the 5′ fragment of Hedgehog Acyltransferase (*HHAT*) on chromosome 1 or to the 3’ fragment of Anoctamin 1 (*ANO1*) on chromosome 11 (Supplemental Table 8). These two fusion events were respectively detected in the primary tumors of LUSC-06 and LUSC-019, and might break the *SET* domain of *SETD3* and result in the inhibition of its tumor suppression function [30]. The actual existence and functions of these fusion genes need further experimental validation.

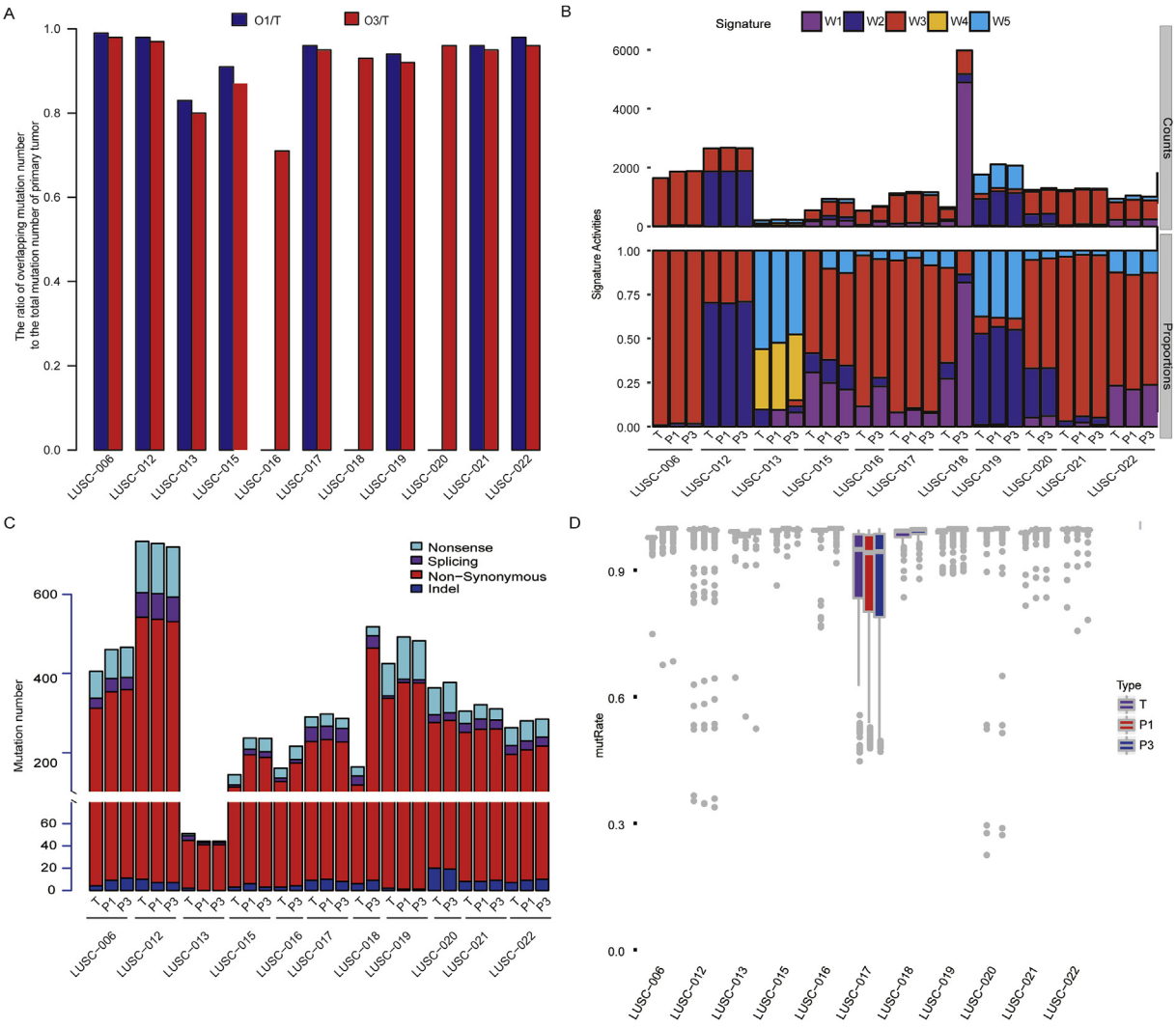

Fig. 1. Homology and heterogeneity of genomic alterations among primary and PDX tumors. A. The ratios of the overlapping mutation number between Passage 1 (P1) or Passage 3 (P3) of PDX tumor and primary tumor (T) (O1 or O3) to the total mutation number of primary tumor (O1/T or O3/T). These two ratios were respectively presented in blue and red colors. B. The counts and proportions of five mutation signatures of primary and corresponding PDX tumor samples remained similar. Five mutation signatures were extracted according to the patterns of base substitutions (W1-W5), and shown in different colors. The x-axis presented the sample ID and the y-axis in upper and lower panels respectively illustrated the counts and proportions of mutation signatures. C. The proportions of various non-synonymous mutation types remained similar among the primary and corresponding PDX tumor samples. The mutation types, including non-synonymous and nonsense SNV, splicing and Indel variants were displayed in different colors. The vertical axis illustrated the mutation number in different samples, and the x-axis presented the sample ID. D. The mutation allele frequencies (MAFs) of non-synonymous somatic mutations corrected for tumor purities in primary and PDX tumors were similar. The MAFs of T, P1 and P3 tumors were presented in different colors. (For interpretation of the references to color in this figure legend, the reader is referred to the Web version of this article.)

3.5. Significant genes verified by target sequencing

A target region captured sequencing (TS) was performed to verify a set of 56 driver genes with relatively high frequencies of SNVs or CNVs detected by WES or WGS in the primary (T) and PDX (P3) tumor and control normal samples of 10 LUSC cases described above, and in the primary tumor and control normal samples of additional 70 LUSC cases. According to the summary in Supplemental Table 10, most of the SNVs detected in the T and P3 samples of 10 LUSC cases by WES were also detected by TS analysis, with only one missing SNV in P3 of LUSC-018 case. Because of the increased sequencing depth in TS analysis, more SNVs were detected in all the tumor samples of 10 LUSC cases compared with WES analysis. The SNVs and CNVs detected in target sequencing were summarized in Supplemental Tables 11 and 12 respectively. Moreover, the 30 genes with highest frequencies of SNV were presented in Fig. 2 with their mutation frequencies and mutation types in 80 tumor samples. And the top 30 CNV genes were shown in Fig. 3 with their variation types in 80 tumor samples. And the numbers of LUSC cases carrying CNVs of those top 30 genes and corresponding CNV frequencies were presented in Supplemental Table 13.

Furthermore, seven genes both in the top 30 lists of SNV and CNV including *GRM1*,*PIK3CG*, *GRM8*, *FGFR2*, *PIK3CA*,*CSMD3* and *ZFHX4*, and two genes only presented in the top 30 CNV list, including *CLDN1* and *RIT1*, were selected as targeting candidates for further validation. Among these 9 candidates, *GRM1, PIK3CG,FGFR2* and *PIK3CA* had been reported to promote tumor progression in multiple types of malignancies [31–36], However, their specific functions in the development of squamous cell lung cancer (LUSC) were necessary to verify. The functions of other 5 genes, *GRM8, CSMD3, ZFHX4, CLDN1* and *RIT1* in malignant progression were much less reported and needed further validation.

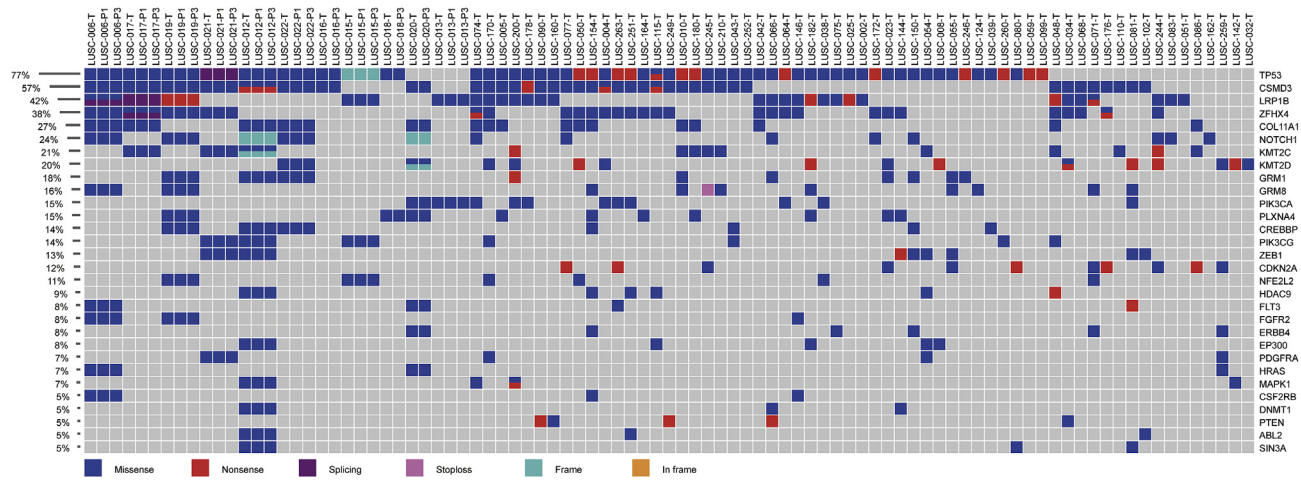

Fig. 2. Significant genes carrying SNVs and verified by targeting sequencing.
The 30 genes with highest frequencies of SNV genes revealed by target sequencing were listed. The sample IDs were showed on the top. The mutation frequencies were displayed on the left, and the gene abbreviations were showed on the right. The icons of mutation types were listed at the bottom in different colors. (For interpretation of the references to color in this figure legend, the reader is referred to the Web version of this article.)

3.6. Functional validation of targeting candidates

The sgRNAs of SaCas9 targeting the 9 candidates were designed using Benchling tool, and respectively cloned into the lentiviral vector expressing SaCas9. The sgRNA efficiencies were confirmed in 293T cells through T7E1 assay (Fig. 4A). The sequences of sgRNAs and PCR primers for T7E1 assay were respectively summarized in Supplemental Table 14 and Supplemental Table 15.

Then the loss of function assays for 9 candidates were conducted in PDX tumor cells carrying corresponding mutations. In detail, *GRM8* was knocked out in LUSC-019 cells. *FGFR2* and *ZFHX4* were individually depleted in LUSC-006 cells. *PIK3CG*, *GRM1* and *CSMD3* were respectively knocked out in LUSC-012 cells. *PIK3CA, CLDN1* and *RIT1* were individually depleted in LUSC-021 cells.

The results of cell viability (Celltiter) and cytotoxicity (LDH) assays both showed that the knock-out of *GRM8, FGFR2, PIK3CG, GRM1, PIK3CA, CLDN1* and *RIT1* were all able to significantly inhibit the survival and induce the death of corresponding PDX tumor cells, and *FGFR2* depletion conferred the strongest effects. In contrast, the depletion of *ZFHX4* and *CSMD3* significantly promoted the survival and inhibited the death of PDX tumor cells (Fig. 4B, Supplemental Fig. 5). Therefore, *GRM8, FGFR2, PIK3CG, GRM1, PIK3CA, CLDN1* and *RIT1* might function to promote the cell survival of squamous cell lung cancer. *ZFHX4* and *CSMD3* might play the roles of tumor suppressor in squamous cell lung cancer.

Metabotropic glutamate receptor 8 (*GRM8*) had both relatively high frequencies of SNVs (16%) and amplification (62.5%) in our LUSC cohort, compared with other validated oncogenic candidates, including

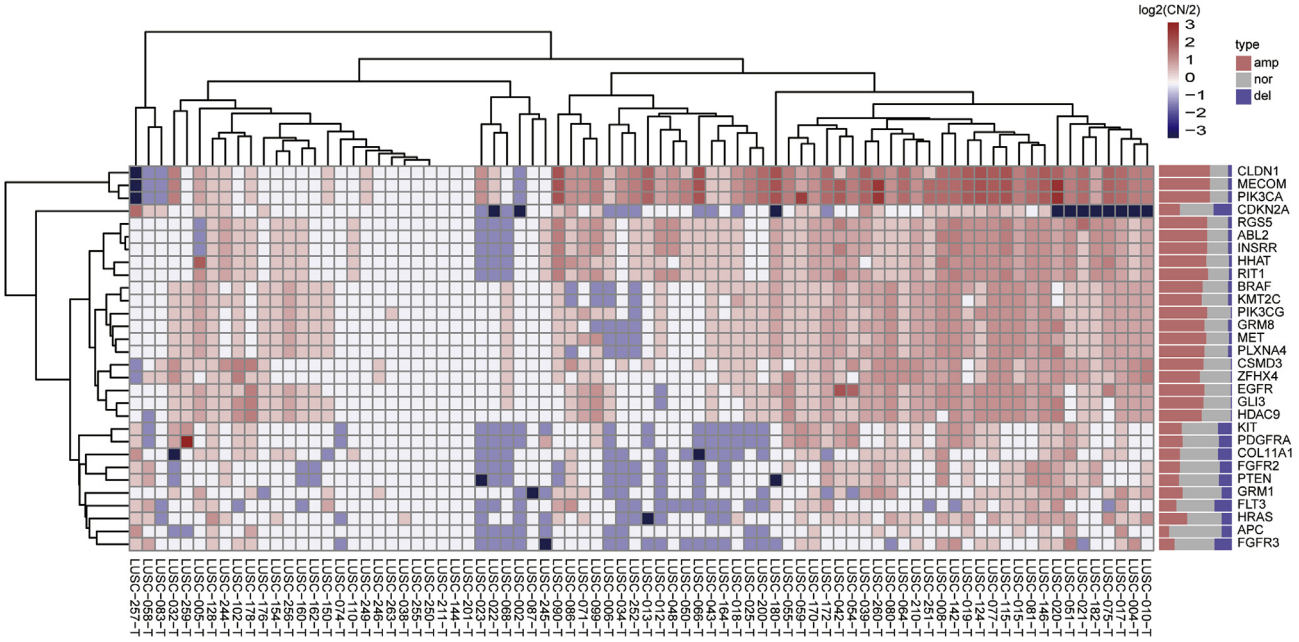

Fig. 3. Significant genes carrying CNVs and verified by targeting sequencing.
The 30 significant genes with highest frequencies of CNVs revealed by target sequencing were listed. The sample IDs were showed at the bottom. The mutation frequencies displayed in bar graph on the right together with the gene abbreviations. The icons of amplification, normal and deletion were displayed on the top. The value of log to the base 2 of copy number (CN) divided by 2 (Log2(CN/2)) were presented in gradually darker colors. (For interpretation of the references to color in this figure legend, the reader is referred to the Web version of this article.)

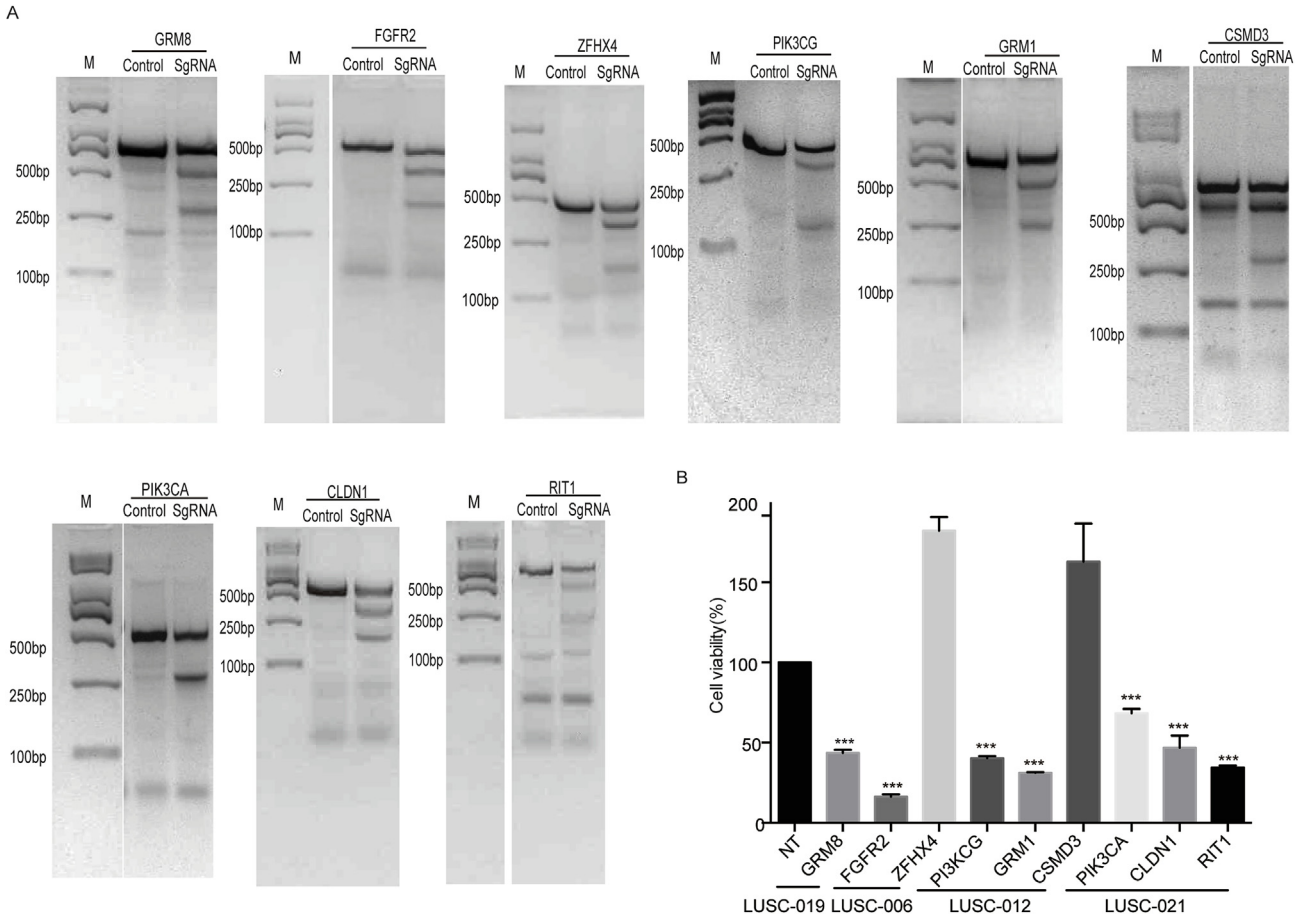

Fig. 4. Functional validation of targeting candidates. A. The sgRNAs targeting 9 candidates could all efficiently induce the cleavages at the targeting points. The loss-of-function lentiviral vectors targeting 9 candidates were respectively transfected in 293T cells, and T7E1 assays were carried out to validate the sgRNA efficiencies. B. The depletions of 9 candidates in the PDX tumor cells carrying corresponding mutations had different effects on cell viability. The PDX cells were infected with lentivirus carrying sgRNAs targeting the indicated genes. The virus packaged by non-targeting vector (NT) served as the control. The star symbols indicated the statistical significance of viability inhibition (***p < 0.001 by unpaired two-tailed *t*-test).

*FGFR2 (*SNV *8%,* Amp *28.75%), PIK3CG (*SNV *14%,* Amp *66.25%), GRM1 (*SNV *18%,* Amp *32.5%), PIK3CA (*SNV *15%,* Amp *70%), CLDN1 (*SNV *0%,* Amp *70%)* and *RIT1 (*SNV *0%,* Amp *67.5%).* Furthermore, the roles of variations of GRM8 in the progression of LUSC were rarely reported and necessary to clarify.

3.7. Transcriptional activation of GRM8 promoted the proliferation of LUSC cells through inhibiting cAMP pathway and activating MAPK pathway

GRM8 is one of the eight members of G-protein coupled receptors for glutamate family. It can couple to a variety of intracellular second messenger systems to modulate neuronal functions, such as neuronal excitability and development. GRM8 was reported to function in mediating the reduction of intracellular cAMP concentration through inhibiting the adenylate cyclase activity [37]. According to the sequencing data of TCGA LUSC cohort (498 cases), the 211 cases with GRM8 amplification also had significantly higher transcription levels of GRM8 compared with the rest cases (P = 0.04). And the transcription level of GRM8 was reversely correlated with the prognosis of LUSC cases (P = 0.019) (Supplemental Fig. 6). These results suggested that the amplification of GRM8 might play a promoting role in LUSC progression.

To further study the function of GRM8 in LUSC cells, GRM8 was transcriptionally activated in LUSC cell-lines EBC-1 and SK-MES-1 through the SAM CRISPRa system. In detail, 4 sgRNAs targeting the promoter region of GRM8 were designed using Benchling tool (Supplemental Table 14) and were individually cloned into the CRISPRa vector. Through co-transfection of the three-vector CRISPRa system respectively expressing sgRNA, mutant SpCas9 (dCas9), and transcription activating domains VP64, P65 and HSF1, the mRNA levels of GRM8 were up-regulated. sgRNA3 was found most efficient (Supplemental Fig. 7). According to the results of CCK8 assay and cell counting, GRM8 activation significantly enhanced the proliferation of EBC-1 cells compared with the non-targeting control (Fig. 5A, Supplemental Fig. 8A). And a concordant phenotype was observed in SK-MES-1 cell (Supplemental Fig. 9A). And GRM8 activation significantly reduced the intracellular cAMP concentration and PKA activity in both cell-lines, revealed by ELISA assay for cAMP measurement and the substrate-phosphorylation assay of PKA (Fig. 5B and C, Supplemantal Fig. 9B and C). According to previous studies, the activation of cAMP pathway would block the activation of MAPK pathway, which was a main intracellular pathway transmitting the proliferation and survival signals [38]. Consistently, the phosphorylation levels of MEK and ERK, key components of MAPK pathway, were significantly enhanced upon GRM8 activation (Fig. 5D, Supplemental Fig. 9D). The underlying bar plots showed the quantification and statistical results of western blot. Our results indicated that GRM8 activation inhibited cAMP pathway, which consequently activated the MAPK pathway. Furthermore, the treatment of cAMP pathway activator, Forskolin, or MAPK pathway inhibitor, Selumetinib, could significantly inhibit the up-regulated phosphorylation of ERK induced by GRM8 activation (Fig. 5E and F, Supplemental Figs. 9E and 9F). While the results of

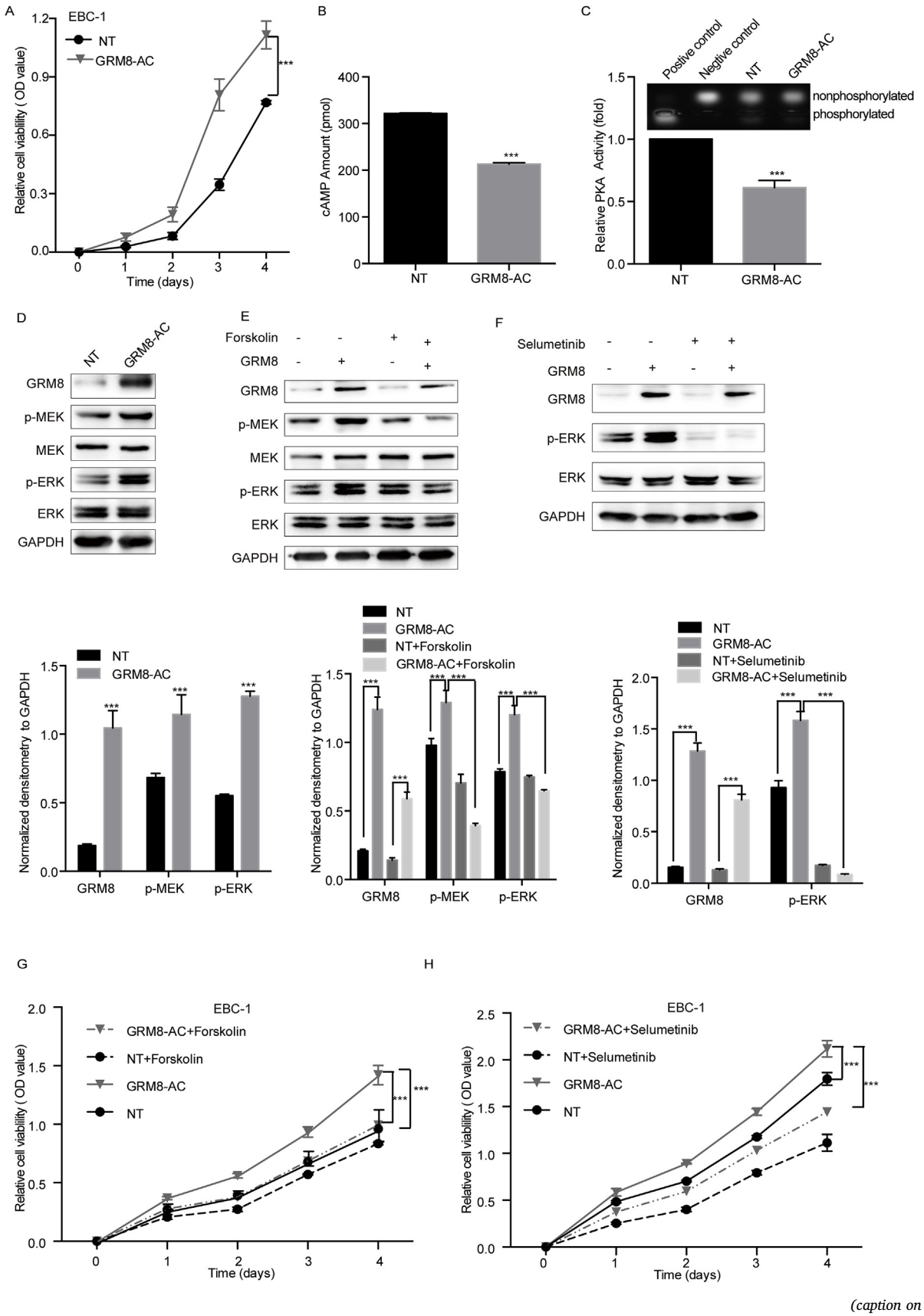

(caption on next page)

Fig. 5. GRM8 activation promoted the proliferation and survival of squamous cell lung cancer. A. GRM8 activation significantly promoted the growth of EBC-1 cells. The cell growth status was measured by CCK-8 assay for 4 days. The square and triangle respectively indicated the non-targeting control and the GRM8 activated cells. Proliferation assay are expressed as the mean ± SD of three replicate assay (***, $p < 0.001$ by two-way ANOVA). B. GRM8 activation decreased the intracellular cAMP level in EBC-1 cell measured by cAMP ELISA assay(***$p < 0.001$ by unpaired two-tailed *t*-test). C. GRM8 activation inhibited the activity of PKA in EBC-1 cell. The upper panel was the representative gel indicating the substrate phosphorylation status. The lower one showed the fold change of PKA activity (***$p < 0.001$ by unpaired two-tailed *t*-test). D. GRM8 activation upregulated the phosphorylations of MEK and ERK. The phosphorylation status of MEK and ERK was detected by Western blot. The level of proteins was quantified by using the software ImageJ and analyzed by unpaired two-tailed *t*-test in underlying graph (***, $p < 0.001$). E-F. The treatments of cAMP activator Forskolin and MEK inhibitor Selumetinib inhibited the phosphorylation of ERK. EBC-1 cells with or without GRM8 activation were respectively treated with 30 μM Forskolin (E) and 2 μM Selumetinib (F) for 2 h before Western blot analysis. The level of proteins was quantified by using the software ImageJ by one-way ANOVA and unpaired two-tailed *t*-test in underlying graph (*, $0.01 < p < 0.05$, **, $0.001 < p < 0.01$, ***, $p < 0.001$). G-H. The treatments of Forskolin and Selumetinib both inhibited the proliferation of EBC-1 cells induced by GRM8 activation. EBC-1 cells with or without GRM8 activation were respectively treated with 200 μM Forskolin (G) and 5 μM Selumetinib (H). And the cell growth status was measured by CCK-8 assay for 4 days(***$p < 0.001$ by two-way ANOVA).

CCK8 and LDH assays both showed that the treatments of Forskolin and Selumetinib could significantly inhibit the GRM8-enhanced proliferation of EBC-1 cells (Fig. 5G and H, Supplemental Figs. 8B and 8C). And concordant phenotypes were also observed in SK-MES-1 cells (Supplemental Figs. 9G and 9H). In summary, the transcriptional activation of GRM8 promoted the proliferation and survival of LUSC tumor cells through inhibiting cAMP pathway and activating MAPK pathway. And the amplification of GRM8 which up-regulated the transcriptional level of GRM8 might be an activating variant of GRM8 and play a promoting role in LUSC progression.

3.8. The SNV resulting in the Alanine/Glycine change at the 112th amino acid (A112G) conferred the activation of GRM8 and induced cell proliferation

GRM8 had SNV frequencies of 16% in our LUSC cohort and of 7.34% in TCGA LUSC cohort. Two cases in our cohort harbored GRM8 mutations, A112G in LUSC-019 and P425T in LUSC-006 respectively. The sanger sequencing on the PCR fragments of cDNA samples of primary tumors from LUSC-019 and LUSC-006 indicated that A112G mutation was well transcribed in tumor sample (Supplemental Fig. 10), While P425T mutation could not be detected by sequencing in cDNA sample, which suggested that P425T might not be well transcribed in corresponding tumor tissue (Data not shown). Therefore, we focused on studying the function of A112G mutation of GRM8. We first constructed A112G mutation in 293T cell with relatively higher constitutive expression level of GRM8 through CRISPR system and homology-directed repair mechanism (HDR) [39] (Fig. 6A), and in LUSC cell-lines EBC-1 and SK-MES-1 with relatively lower constitutive expression levels through exogenously expressing the mutant protein. The sequences of sgRNA and ssDNA, and the PCR primers for sequencing were listed in Supplemental Table 16. According to the cell proliferation assay, A112G robustly induced the proliferation of 293T cell and LUSC cells compared with the wild-type control (Fig. 6B and E, Supplemental Fig. 11A). As mentioned above, GRM8 inhibited cAMP/PKA and activated MAPK signaling pathways, so we detected the PKA kinase activities and MEK/ERK phosphorylations in the mutated cells. A112G significantly suppressed the PKA activities and up-regulated the phosphorylations of MEK and ERK in 293T cell and two LUSC cell-lines, indicating that this mutation conferred activation to GRM8 (Fig. 6C, D, 6F and 6G, Supplemental Figs. 11B and 11C). Therefore, the A112G mutation might be also an activating variant of GRM8 and play a promoting role in LUSC progression.

3.9. cAMP activator and MEK inhibitor could become a potential therapeutic strategy in LUSC tumors carrying GRM8-activating mutations

To determine if the activation of cAMP/PKA and MAPK signal pathway was responsible for GRM8-activating mutation (A112G) induced proliferation, we assayed the pathway status and the proliferation of 293T cell and LUSC cell-line EBC-1 in the presence or absence of cAMP activator and MEK inhibitor. The treatments of cAMP pathway activator, Forskolin, or MAPK pathway inhibitor, Selumetinib, could significantly inhibit the phosphorylation of ERK up-regulated in the cells with A112G mutation of GRM8 (Fig. 7A,C, E and G) and the cell proliferation induced by corresponding GRM8 mutation (Fig. 7B, D, F and H). Furthermore, either Forskolin or Selumetinib treatment could inhibit the survival of PDX tumor cell of LUSC-019 harboring both amplification and A112G mutation of GRM8. The inhibition effect of Forskolin was dose-dependent and more significant than that of Selumetinib. Combined treatments of Forskolin and Selumetinib showed additive inhibition effects on PDX tumor cells (Fig. 8A). All the data indicated that the GRM8 activating variants including amplification and A112G mutation promoted the cell proliferation through inhibiting cAMP/PKA pathway and stimulating MAPK pathway (Fig. 8B) and suggested that targeting the components of GRM8 signaling pathway including cAMP and MEK could become a potential therapeutic strategy in LUSC tumors carrying GRM8-activating variants.

4. Discussion

Through the integrated analysis of genomic sequencing and CRISPR-Cas9 genome editing, a group of potential driver genes carrying consistent somatic mutations among the primary and PDX tumor samples were identified and validated. Further study elucidated that GRM8 promoted the survival of LUSC tumor cells through inhibiting cAMP pathway and activating MAPK pathway. The SNV identified in LUSC tumors, A112G, activated GRM8 and promoted cell proliferation. Furthermore, cAMP activator and MEK inhibitor could significantly block the cell proliferation and survival of LUSC tumor cells with GRM8 mutations. Therefore, the GRM8 signaling pathway could potentially serve as promising therapeutic targets of squamous cell lung cancer carrying GRM8-activating mutations.

Previous studies had described the successful establishment of PDX models of lung cancer, and the PDX tumor maintained the histological and molecular features of primary tumor after a series of passages [30,40]. According to the WES data, the rates of overlapping mutations ranged from 0.71 to 0.99. More importantly, the mutation types and signatures were very similar among the primary and PDX samples. These results indicate that the molecular features maintained consistent among the primary and PDX tumors of our sample cohort. And our LUSC PDX models can be widely applied for the validation of potential therapeutic targets and strategies.

The candidate selection process was optimized through combining the driver gene screening and mutation frequency analysis. The iCAGES tool and COSMIC database were utilized to screen the potential driver genes from WES and WGS data. Around 300 potential driver genes carrying SNVs were identified by iCAGES from WES data, while 142 potential driver genes carrying CNVs were identified from WGS data according to COSMIC database and previous publications. The 42 genes frequently mutated both in our cohort and TCGA cohorts were also combined in case of missing novel candidates. Furthermore, 56 genes carrying highly frequent SNVs and/or CNVs were verified through target region captured sequencing both in the samples for WES and

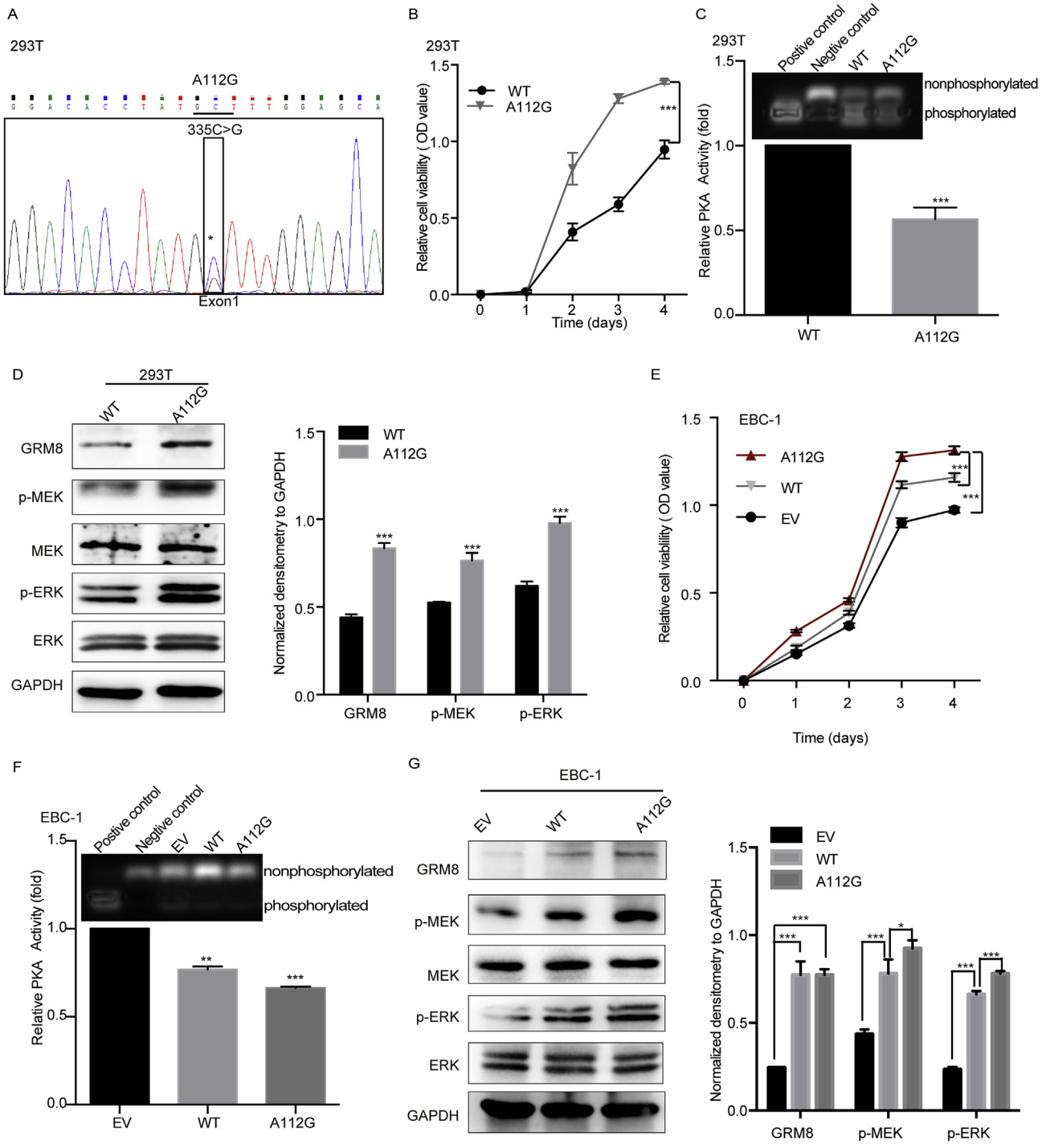

Fig. 6. The A112G mutation of GRM8 induced cell proliferation and regulated c-AMP/PKA and MEK/ERK signaling pathways in 293T cells andEBC-1 cells. A. Sanger sequencing results of PCR products amplifying the mutation in the Exon1of GRM8 from the 293T cell-line containing corresponding mutation. The black boxes indicated the position of A112G point mutation. B and E. A112G mutation of GRM8 significantly promoted the proliferation of 293T cells and EBC-1 cells. The growth status of mutated cells was measured by CCK-8 assay for 4 days. Proliferation assay are expressed as the mean ± SD of three replicate assay (***, $p < 0.001$ by two-way ANOVA). C and F. A112G mutations of GRM8 inhibited the activities of PKA (***$p < 0.001$ by unpaired two-tailed *t*-test). D and G. GRM8 mutations upregulated the phosphorylations of MEK and ERK. The phosphorylation status of MEK and ERK was detected by Western blot. The level of proteins was quantified using the software ImageJ and analyzed by one-way ANOVA and unpaired two-tailed *t*-test in underlying graph(*, $0.01 < p < 0.05$, **, $0.001 < p < 0.01$, ***, $p < 0.001$).

WGS analysis, and in the tumor samples of additional 70 LUSC cases. Based on the verification of target sequencing, seven genes carrying both highly frequent SNV and CNV, including *GRM1*,*PIK3CG*, *GRM8*, *FGFR2*, *PIK3CA*,*CSMD3* and *ZFHX4*, and two genes only presented in the top CNV list, including *CLDN1* and *RIT1*, were selected for further functional validation.

The correlations among the overall survival times of TCGA LUSC cohort and the occurrences of non-synonymous mutations of the above 7 candidates (*GRM1*, *PIK3CG*, *GRM8*, *FGFR2*, *PIK3CA*,*CSMD3* and *ZFHX4)* were respectively analyzed through Kaplan-Meier survival

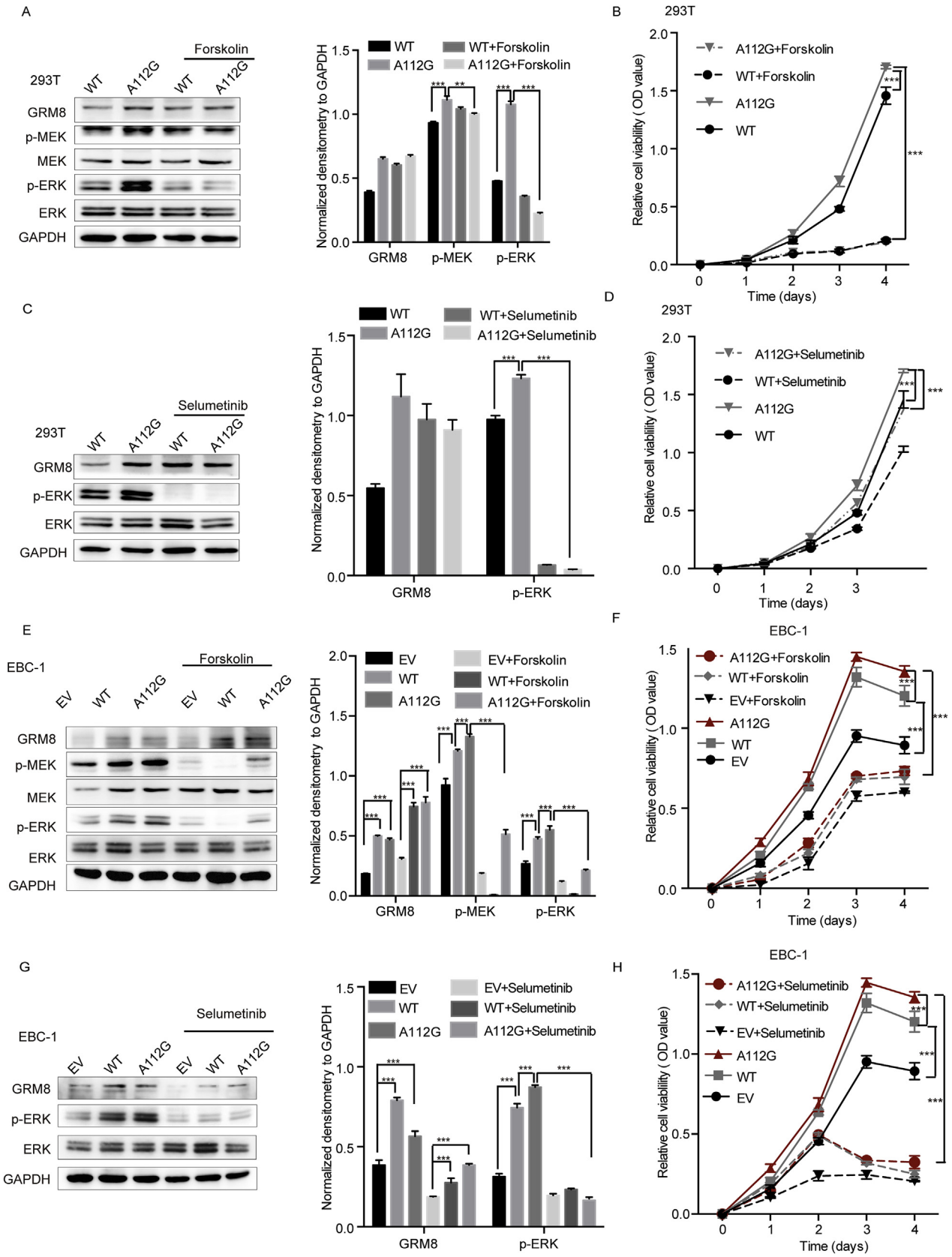

Fig. 7. The cAMP activator and MEK inhibitor could inhibit the survival of cells carrying A112G mutation of GRM8. A, C, E, G. The treatments of cAMP activator Forskolin and MEK inhibitor Selumetinib inhibited the phosphorylation of ERK in GRM8 mutated 293 and EBC-1 cells. The mutated 293T and EBC-1 cells were respectively treated with 20 μM and 30 μM Forskolin and 10 μM and 2 μM Selumetinib for 2 h before Western blot analysis. The level of protein was quantified using the software ImageJ and analyzed by one-way ANOVA in underlying graph(*, $0.01 < p < 0.05$, **, $0.001 < p < 0.01$, ***, $p < 0.001$). B, D, F, H. The treatments of Forskolin and Selumetinib both inhibited the proliferation of 293T and EBC-1 cells induced by GRM8 point mutation. The 293T and EBC-1 cells with A112G mutations of GRM8 were respectively treated with 100 μM and 200 μM Forskolin, and 10 μM and 5 μM Selumetinib. And the cell growth status was measured by CCK-8 assay for 4 days. (***, $p < 0.001$ by two-way ANOVA).

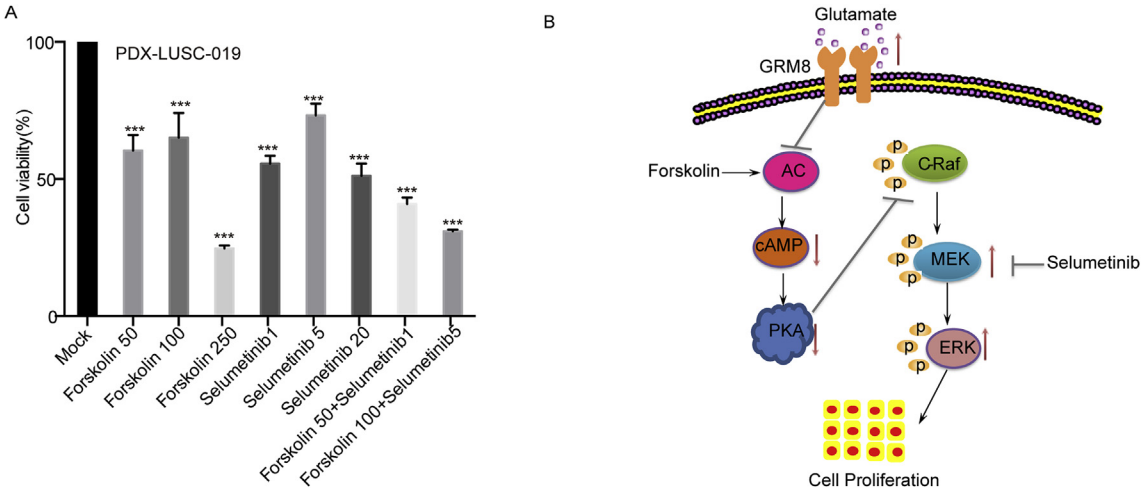

Fig. 8. The cAMP activator and MEK inhibitor could inhibit the survival of PDX tumor cells carrying GRM8-activating mutations. A. The combining treatments of Forskolin and Selumetinib had additive inhibition effects on the viability of PDX tumor cell of LUSC-019 case. The tumor cells were treated with indicated concentrations (uM) of reagents for 72 h. The viability assay was conducted using CellTiter kit (***, $p < 0.001$ by two-way ANOVA). B. GRM8 activation promoted the proliferation of LUSC cells through inhibiting cAMP pathway and activating MAPK pathway. The black arrow line indicated the activating function, and the red block line indicated the inhibiting function. The red arrow line upwards and downwards respectively indicated the activation and inactivation status. (For interpretation of the references to color in this figure legend, the reader is referred to the Web version of this article.)

analysis. All the correlations were statistically insignificant ($P > 0.05$). Usually a large part of non-synonymous mutations detected in a specific gene are not biologically functional. Therefore, further functional studies need be carried out to identify and characterize the specific mutations of the above candidates regulating the progression of LUSC.

Several studies involve the high-throughput screening of cancer driver genes *in vitro* and *in vivo* using CRISPR-Cas9 loss-of-function or gain-of-function systems. For example, Chen et al. mutagenized a non-metastatic mouse cancer cell-line using a genome-scale CRISPR library of loss of function. The mutant cell pool rapidly generated lung metastasis when transplanted into immunocompromised mice. And a small set of genes inhibiting cancer metastasis were identified by sequencing the metastatic tumors [41]. However, all of these screening studies aim at cancer cell-lines, not PDX tumor cells. Since PDX models maintain the pathological and molecular features of clinical samples, the gene function study in PDX tumor cells could potentially provide more information. With 9 candidates successfully validated, our work was the first functional screening of driver genes in PDX tumor cells using CRISPR system. Our system can be extensively applied to more mutation candidates for the identification of effective therapeutic targets.

GRM8 belongs to one of the 8 members of G-protein coupled receptors for glutamate family, and couples to a variety of intracellular second messenger systems to modulate neuronal functions, such as neuronal excitability and development [42]. GRM1, another member of this family, was reported as an oncogene and frequently mutated in various malignancies [32]. Our study and previous report both showed that GRM8 had high SNV frequencies in LUSC tumor samples [43]. And GRM8 was also identified to carry highly frequent amplification in our LUSC cohort. GRM8 was reported to mediate the reduction of intracellular cAMP concentration through inhibiting the adenylate cyclase activity [37]. Recent reports demonstrated that GRM8 inhibited the viabilities of endometrial cancer, neuroblastoma and glioma cells, and increased chemo-sensitivity of neuroblastoma and glioma cells [44–46]. However, the roles of GRM8 and its mutations in the progression of LUSC still remained unclear.

In this report, we found that in TCGA data GRM8 amplification significantly correlated with higher transcription level of GRM8 ($P = 0.04$). And the transcription level of GRM8 was reversely correlated with the prognosis of LUSC cases ($P = 0.019$). The transcriptional up-regulation and A112G mutation of GRM8 significantly promoted the proliferation and survival of LUSC tumor cells through inhibiting cAMP pathway and activating MAPK pathway accordingly. Stimulating cAMP pathway and blocking MAPK pathway could both inhibit the survival of PDX tumor cells containing GRM8 amplification and A112G mutation, and the joint regulation of both pathways could lead to more significant inhibition effect. Although cAMP and MAPK pathways were considered as separated signalings, there was crosstalk between these two pathways in the regulation of cell proliferation [38]. cAMP signaling could regulate MAPK signaling in a cell-type specific manner, which depends on the activation of a GTPase RAP1 by PKA, and on the expression of BRAF. Once activated, RAP1 could inhibit RAS/RAF1/MEK/ERK signaling through blocking the activation of RAF1 by RAS when the expression level of BRAF is low. On the contrary, when the expression of BRAF is up-regulated, RAP1 could activate BRAF and inhibit RAF1 at the same time, resulting in a net effect of ERK activation. According to the TCGA RNA-Seq results, the expression of BRAF keeps at relatively low level in LUSC cell-lines including EBC-1 and SK-MES-1 which were utilized in our study (Data not shown). Therefore, the inhibition of cAMP induced by GRM8 could activate MAPK signaling in lung cancer cells without BRAF activation.

On the other hand, previous reports and our study demonstrated distinct functions of GRM8 in different types of cancer cells, such as tumor suppressing roles in endometrial cancer, neuroblastoma and glioma cells [44–46], and tumor promoting role in LUSC. The cell-type dependent functions of GRM8 might result from the differential status of its downstream cAMP/PKA signaling. cAMP/PKA pathway was commonly considered as a tumor-suppressive signaling, and reported to induce the apoptosis and inhibit the invasion of cancer cells [47,48]. However, when the downstream key effector of cAMP/PKA signaling, CREBBP developed loss-of-function mutations, the function of cAMP/PKA signaling would be dysregulated to promote cancer progression [49]. Since GRM8 played oncogenic role through inhibiting cAMP pathway, the loss-of-function mutations of cAMP/PKA signaling in specific cancer types might transform the role of GRM8 to tumor suppressor. Without question, there might be various factors affecting GRM8 function. Therefore, further studies need be implemented to explore the mediators responsible for the transition of opposite roles of GRM8 in the tumor progression.

As shown in Uniprot database, the activating SNV of GRM8, A112G, identified in our LUSC cohort, localized at the first extracellular domain of GRM8 (Amino acid (aa) 34–853), adjacent to the glutamate binding site at aa156. Based on our report, the overexpression of A112G

mutated GRM8 could both significantly activate MAPK signaling and promote the proliferations of LUSC cell-lines, EBC-1 and SK-MES-1. Moreover, the treatment of mGluR8 specific ligand, (S)-3,4-DCPG had no effect on the proliferation of EBC-1 cell overexpressing mutant GRM8, although it could significantly enhance the proliferation of control EBC-1 cell (Data not shown). These results implied that A112G mutation might be a constitutively activating mutation. The detailed mechanism of A112G-induced activation of GRM8 needs further investigation.

In summary, the integration of genome sequencing and editing on the primary and PDX tumors identified and validated the tumor-promoting function of GRM8 in LUSC. And the LUSC patients carrying GRM8 amplification and A112G mutation might become the intervention objectives targeting the components of GRM8 signaling pathway, including cAMP signaling and MAPK signaling. The mutations of key members of these two signalings, such as BRAF and CREBBP might be also explored to ensure the intervention effect.

Conflicts of interest

The authors have no conflicts of interest to declare.

Acknowledgement

We thank Dr. Jun Wu from Salk Institute for Biological Studies for reading the manuscript and providing helpful comments. This work was supported by the grants from National Key Research and Development Program of China (No. 2016YFC0902301), National Natural Science Foundation of China (No. 81772494 and No. 81502578), Beijing Municipal Administration of Hospitals Clinical Medicine Development of Special Funding Support (ZYLX201509), Peking University 985 Special Funding for Collaborative Research with PKU Hospitals (2013-5-05), and Shenzhen Peacock Plan (No. KQTD20150330171505310), Shenzhen Municipal Government of China (No. JCYJ20170817145218948). This work was also supported by Guangdong Provincial Key Laboratory of Genome Read and Write (No. 2017B030301011), and Shenzhen Engineering Laboratory for Innovative Molecular Diagnostics (DRC-SZ[2016]884).

Appendix A. Supplementary data

Supplementary data to this article can be found online at https://doi.org/10.1016/j.canlet.2018.10.035.

References

[1] R.L. Siegel, K.D. Miller, A. Jemal, Cancer statistics, 2015, Ca - Cancer J. Clin. 65 (2015) 5–29.
[2] D.S. Shames, Wistuba II, The evolving genomic classification of lung cancer, J. Pathol. 232 (2014) 121–133.
[3] E. Shtivelman, T. Hensing, G.R. Simon, P.A. Dennis, G.A. Otterson, R. Bueno, R. Salgia, Molecular pathways and therapeutic targets in lung cancer, Oncotarget 5 (2014) 1392–1433.
[4] H. Gao, J.M. Korn, S. Ferretti, J.E. Monahan, Y. Wang, M. Singh, C. Zhang, C. Schnell, G. Yang, Y. Zhang, O.A. Balbin, S. Barbe, H. Cai, F. Casey, S. Chatterjee, D.Y. Chiang, S. Chuai, S.M. Cogan, S.D. Collins, E. Dammassa, N. Ebel, M. Embry, J. Green, A. Kauffmann, C. Kowal, R.J. Leary, J. Lehar, Y. Liang, A. Loo, E. Lorenzana, E. Robert McDonald 3rd, M.E. McLaughlin, J. Merkin, R. Meyer, T.L. Naylor, M. Patawaran, A. Reddy, C. Roelli, D.A. Ruddy, F. Salangsang, F. Santacroce, A.P. Singh, Y. Tang, W. Tinetto, S. Tobler, R. Velazquez, K. Venkatesan, F. Von Arx, H.Q. Wang, Z. Wang, M. Wiesmann, D. Wyss, F. Xu, H. Bitter, P. Atadja, E. Lees, F. Hofmann, E. Li, N. Keen, R. Cozens, M.R. Jensen, N.K. Pryer, J.A. Williams, W.R. Sellers, High-throughput screening using patient-derived tumor xenografts to predict clinical trial drug response, Nat. Med. 21 (2015) 1318–1325.
[5] O. Shalem, N.E. Sanjana, E. Hartenian, X. Shi, D.A. Scott, T. Mikkelson, D. Heckl, B.L. Ebert, D.E. Root, J.G. Doench, F. Zhang, Genome-scale CRISPR-Cas9 knockout screening in human cells, Science 343 (2014) 84–87.
[6] S. Konermann, M.D. Brigham, A.E. Trevino, J. Joung, O.O. Abudayyeh, C. Barcena, P.D. Hsu, N. Habib, J.S. Gootenberg, H. Nishimasu, O. Nureki, F. Zhang, Genome-scale transcriptional activation by an engineered CRISPR-Cas9 complex, Nature 517 (2015) 583–588.
[7] C. Dong, Y. Guo, H. Yang, Z. He, X. Liu, K. Wang, iCAGES: integrated CAncer GEnome Score for comprehensively prioritizing driver genes in personal cancer genomes, Genome Med. 8 (2016) 135.
[8] J.D. Campbell, A. Alexandrov, J. Kim, J. Wala, A.H. Berger, C.S. Pedamallu, S.A. Shukla, G. Guo, A.N. Brooks, B.A. Murray, M. Imielinski, X. Hu, S. Ling, R. Akbani, M. Rosenberg, C. Cibulskis, A. Ramachandran, E.A. Collisson, D.J. Kwiatkowski, M.S. Lawrence, J.N. Weinstein, R.G. Verhaak, C.J. Wu, P.S. Hammerman, A.D. Cherniack, G. Getz, M.N. Artyomov, R. Schreiber, R. Govindan, M. Meyerson, Distinct patterns of somatic genome alterations in lung adenocarcinomas and squamous cell carcinomas, Nat. Genet. 48 (2016) 607–616.
[9] S.A. Forbes, D. Beare, P. Gunasekaran, K. Leung, N. Bindal, H. Boutselakis, M. Ding, S. Bamford, C. Cole, S. Ward, C.Y. Kok, M. Jia, T. De, J.W. Teague, M.R. Stratton, U. McDermott, P.J. Campbell, COSMIC: exploring the world's knowledge of somatic mutations in human cancer, Nucleic Acids Res. 43 (2015) D805–D811.
[10] J. Huang, X. Liang, Y. Xuan, C. Geng, Y. Li, H. Lu, S. Qu, X. Mei, H. Chen, T. Yu, N. Sun, J. Rao, J. Wang, W. Zhang, Y. Chen, S. Liao, H. Jiang, X. Liu, Z. Yang, F. Mu, S. Gao, A reference human genome dataset of the BGISEQ-500 sequencer, GigaScience 6 (2017) 1–9.
[11] R. Li, C. Yu, Y. Li, T.W. Lam, S.M. Yiu, K. Kristiansen, J. Wang, SOAP2: an improved ultrafast tool for short read alignment, Bioinformatics 25 (2009) 1966–1967.
[12] H. Li, R. Durbin, Fast and accurate short read alignment with Burrows-Wheeler transform, Bioinformatics 25 (2009) 1754–1760.
[13] picard, in.
[14] A. Tarasov, A.J. Vilella, E. Cuppen, I.J. Nijman, P. Prins, Sambamba: fast processing of NGS alignment formats, Bioinformatics 31 (2015) 2032–2034.
[15] W. Zhou, H. Zhao, Z. Chong, R.J. Mark, A.K. Eterovic, F. Meric-Bernstam, K. Chen, ClinSeK: a targeted variant characterization framework for clinical sequencing, Genome Med. 7 (2015) 34.
[16] M.A. DePristo, E. Banks, R. Poplin, K.V. Garimella, J.R. Maguire, C. Hartl, A.A. Philippakis, G. del Angel, M.A. Rivas, M. Hanna, A. McKenna, T.J. Fennell, A.M. Kernytsky, A.Y. Sivachenko, K. Cibulskis, S.B. Gabriel, D. Altshuler, M.J. Daly, A framework for variation discovery and genotyping using next-generation DNA sequencing data, Nat. Genet. 43 (2011) 491–498.
[17] Y. Fan, L. Xi, D.S. Hughes, J. Zhang, J. Zhang, P.A. Futreal, D.A. Wheeler, W. Wang, MuSE: accounting for tumor heterogeneity using a sample-specific error model improves sensitivity and specificity in mutation calling from sequencing data, Genome Biol. 17 (2016) 178.
[18] A. Rimmer, H. Phan, I. Mathieson, Z. Iqbal, S.R.F. Twigg, W.G.S. Consortium, A.O.M. Wilkie, G. McVean, G. Lunter, Integrating mapping-, assembly- and haplotype-based approaches for calling variants in clinical sequencing applications, Nat. Genet. 46 (2014) 912–918.
[19] D.E. Larson, T.E. Abbott, R.K. Wilson, Using SomaticSniper to detect somatic single nucleotide variants, Current protocols in bioinformatics 45 (2014) 15 15 11–18.
[20] E. Reble, C.A. Castellani, M.G. Melka, R. O'Reilly, S.M. Singh, VarScan2 analysis of de novo variants in monozygotic twins discordant for schizophrenia, Psychiatr. Genet. 27 (2017) 62–70.
[21] M. Josephidou, A.G. Lynch, S. Tavare, multiSNV: a probabilistic approach for improving detection of somatic point mutations from multiple related tumour samples, Nucleic Acids Res. 43 (2015) e61.
[22] R. Shen, V.E. Seshan, FACETS: allele-specific copy number and clonal heterogeneity analysis tool for high-throughput DNA sequencing, Nucleic Acids Res. 44 (2016) e131.
[23] Z. Chong, J. Ruan, M. Gao, W. Zhou, T. Chen, X. Fan, L. Ding, A.Y. Lee, P. Boutros, J. Chen, K. Chen, novoBreak: local assembly for breakpoint detection in cancer genomes, Nat. Methods 14 (2017) 65–67.
[24] D. L.et al., bam-readcount, in.
[25] A. Roth, J. Khattra, D. Yap, A. Wan, E. Laks, J. Biele, G. Ha, S. Aparicio, A. Bouchard-Cote, S.P. Shah, PyClone: statistical inference of clonal population structure in cancer, Nat. Methods 11 (2014) 396–398.
[26] A. Subramanian, P. Tamayo, V.K. Mootha, S. Mukherjee, B.L. Ebert, M.A. Gillette, A. Paulovich, S.L. Pomeroy, T.R. Golub, E.S. Lander, J.P. Mesirov, Gene set enrichment analysis: a knowledge-based approach for interpreting genome-wide expression profiles, Proc. Natl. Acad. Sci. U. S. A. 102 (2005) 15545–15550.
[27] L.B. Alexandrov, S. Nik-Zainal, D.C. Wedge, S.A. Aparicio, S. Behjati, A.V. Biankin, G.R. Bignell, N. Bolli, A. Borg, A.L. Borresen-Dale, S. Boyault, B. Burkhardt, A.P. Butler, C. Caldas, H.R. Davies, C. Desmedt, R. Eils, J.E. Eyfjord, J.A. Foekens, M. Greaves, F. Hosoda, B. Hutter, T. Ilicic, S. Imbeaud, M. Imielinski, N. Jager, D.T. Jones, D. Jones, S. Knappskog, M. Kool, S.R. Lakhani, C. Lopez-Otin, S. Martin, N.C. Munshi, H. Nakamura, P.A. Northcott, M. Pajic, E. Papaemmanuil, A. Paradiso, J.V. Pearson, X.S. Puente, K. Raine, M. Ramakrishna, A.L. Richardson, J. Richter, P. Rosenstiel, M. Schlesner, T.N. Schumacher, P.N. Span, J.W. Teague, Y. Totoki, A.N. Tutt, R. Valdes-Mas, M.M. van Buuren, L. van 't Veer, A. Vincent-Salomon, N. Waddell, L.R. Yates, I. Australian Pancreatic Cancer Genome, I.B.C. Consortium, I.M.-S. Consortium, I. PedBrain, J. Zucman-Rossi, P.A. Futreal, U. McDermott, P. Lichter, M. Meyerson, S.M. Grimmond, R. Siebert, E. Campo, T. Shibata, S.M. Pfister, P.J. Campbell, M.R. Stratton, Signatures of mutational processes in human cancer, Nature 500 (2013) 415–421.
[28] J. Kim, K.W. Mouw, P. Polak, L.Z. Braunstein, A. Kamburov, D.J. Kwiatkowski, J.E. Rosenberg, E.M. Van Allen, A. D'Andrea, G. Getz, Somatic ERCC2 mutations are associated with a distinct genomic signature in urothelial tumors, Nat. Genet. 48 (2016) 600–606.
[29] J.D. Campbell, A. Alexandrov, J. Kim, J. Wala, A.H. Berger, C.S. Pedamallu, S.A. Shukla, G. Guo, A.N. Brooks, B.A. Murray, M. Imielinski, X. Hu, S. Ling, R. Akbani, M. Rosenberg, C. Cibulskis, A. Ramachandran, E.A. Collisson, D.J. Kwiatkowski, M.S. Lawrence, J.N. Weinstein, R.G. Verhaak, C.J. Wu,

P.S. Hammerman, A.D. Cherniack, G. Getz, N. Cancer Genome Atlas Research, M.N. Artyomov, R. Schreiber, R. Govindan, M. Meyerson, Distinct patterns of somatic genome alterations in lung adenocarcinomas and squamous cell carcinomas, Nat. Genet. 48 (2016) 607–616.

[30] Z. Chen, C.T. Yan, Y. Dou, S.S. Viboolsittiseri, J.H. Wang, The role of a newly identified SET domain-containing protein, SETD3, in oncogenesis, Haematologica 98 (2013) 739–743.

[31] Y. Zhang, W. Xu, H. Guo, Y. He, S.H. Lee, X. Song, X. Li, Y. Guo, Y. Zhao, C. Ding, F. Ning, Y. Ma, Q.Y. Lei, X. Hu, S. Li, W. Guo, NOTCH1 signaling regulates self-renewal and platinum chemoresistance of cancer stem-like cells in human non-small cell lung cancer, Cancer Res. 77 (2017) 3082–3091.

[32] J.J. Martino, B.A. Wall, E. Mastrantoni, B.J. Wilimczyk, S.N. La Cava, K. Degenhardt, E. White, S. Chen, Metabotropic glutamate receptor 1 (Grm1) is an oncogene in epithelial cells, Oncogene 32 (2013) 4366–4376.

[33] S. Chen, F. Li, H. Chai, X. Tao, H. Wang, A. Ji, miR-502 inhibits cell proliferation and tumor growth in hepatocellular carcinoma through suppressing phosphoinositide 3-kinase catalytic subunit gamma, Biochem. Biophys. Res. Commun. 464 (2015) 500–505.

[34] L. Xie, X. Su, L. Zhang, X. Yin, L. Tang, X. Zhang, Y. Xu, Z. Gao, K. Liu, M. Zhou, B. Gao, D. Shen, J. Ji, P.R. Gavine, J. Zhang, E. Kilgour, Q. Ji, FGFR2 gene amplification in gastric cancer predicts sensitivity to the selective FGFR inhibitor AZD4547, Clin. Canc. Res. 19 (2013) 2572–2583.

[35] H. Lei, C.X. Deng, Fibroblast growth factor receptor 2 signaling in breast cancer, Int. J. Biol. Sci. 13 (2017) 1163–1171.

[36] D.A. Fruman, H. Chiu, B.D. Hopkins, S. Bagrodia, L.C. Cantley, R.T. Abraham, The PI3K pathway in human disease, Cell 170 (2017) 605–635.

[37] M. Rose, E. Dutting, R. Enz, Band 4.1 proteins are expressed in the retina and interact with both isoforms of the metabotropic glutamate receptor type 8, J. Neurochem. 105 (2008) 2375–2387.

[38] P.J. Stork, J.M. Schmitt, Crosstalk between cAMP and MAP kinase signaling in the regulation of cell proliferation, Trends Cell Biol. 12 (2002) 258–266.

[39] C.D. Richardson, G.J. Ray, M.A. DeWitt, G.L. Curie, J.E. Corn, Enhancing homology-directed genome editing by catalytically active and inactive CRISPR-Cas9 using asymmetric donor DNA, Nat. Biotechnol. 34 (2016) 339–344.

[40] C. Hao, L. Wang, S. Peng, M. Cao, H. Li, J. Hu, X. Huang, W. Liu, H. Zhang, S. Wu, A. Pataer, J.V. Heymach, A.K. Eterovic, Q. Zhang, K.R. Shaw, K. Chen, A. Futreal, M. Wang, W. Hofstetter, R. Mehran, D. Rice, J.A. Roth, B. Sepesi, S.G. Swisher, A. Vaporciyan, G.L. Walsh, F.M. Johnson, B. Fang, Gene mutations in primary tumors and corresponding patient-derived xenografts derived from non-small cell lung cancer, Cancer Lett. 357 (2015) 179–185.

[41] S. Chen, N.E. Sanjana, K. Zheng, O. Shalem, K. Lee, X. Shi, D.A. Scott, J. Song, J.Q. Pan, R. Weissleder, H. Lee, F. Zhang, P.A. Sharp, Genome-wide CRISPR screen in a mouse model of tumor growth and metastasis, Cell 160 (2015) 1246–1260.

[42] A. Stepulak, R. Rola, K. Polberg, C. Ikonomidou, Glutamate and its receptors in cancer, J. Neural. Transm. 121 (2014) 933–944.

[43] M. Choi, H. Kadara, J. Zhang, E.R. Parra, J. Rodriguez-Canales, S.G. Gaffney, Z. Zhao, C. Behrens, J. Fujimoto, C. Chow, K. Kim, N. Kalhor, C. Moran, D. Rimm, S. Swisher, D.L. Gibbons, J. Heymach, E. Kaftan, J.P. Townsend, T.J. Lynch, J. Schlessinger, J. Lee, R.P. Lifton, R.S. Herbst, Wistuba II, Mutation profiles in early-stage lung squamous cell carcinoma with clinical follow-up and correlation with markers of immune function, Ann. Oncol. 28 (2017) 83–89.

[44] D. Jantas, B. Grygier, S. Golda, J. Chwastek, J. Zatorska, M. Tertil, An endogenous and ectopic expression of metabotropic glutamate receptor 8 (mGluR8) inhibits proliferation and increases chemosensitivity of human neuroblastoma and glioma cells, Cancer Lett. 432 (2018) 1–16.

[45] D. Jantas, B. Grygier, J. Zatorska, W. Lason, Allosteric and orthosteric activators of mGluR8 differentially affect the chemotherapeutic-induced human neuroblastoma SH-SY5Y cell damage: the impact of cell differentiation state, Basic Clin. Pharmacol. Toxicol. 123 (2018) 443–450.

[46] H. Liang, L.W. Cheung, J. Li, Z. Ju, S. Yu, K. Stemke-Hale, T. Dogruluk, Y. Lu, X. Liu, C. Gu, W. Guo, S.E. Scherer, H. Carter, S.N. Westin, M.D. Dyer, R.G. Verhaak, F. Zhang, R. Karchin, C.G. Liu, K.H. Lu, R.R. Broaddus, K.L. Scott, B.T. Hennessy, G.B. Mills, Whole-exome sequencing combined with functional genomics reveals novel candidate driver cancer genes in endometrial cancer, Genome Res. 22 (2012) 2120–2129.

[47] P.A. Insel, A. Wilderman, L. Zhang, M.M. Keshwani, A.C. Zambon, Cyclic AMP/PKA-promoted apoptosis: insights from studies of S49 lymphoma cells, Horm. Metab. Res. 46 (2014) 854–862.

[48] Y. Ou, X. Zheng, Y. Gao, M. Shu, T. Leng, Y. Li, W. Yin, W. Zhu, Y. Huang, Y. Zhou, J. Tang, P. Qiu, G. Yan, J. Hu, H. Ruan, H. Hu, Activation of cyclic AMP/PKA pathway inhibits bladder cancer cell invasion by targeting MAP4-dependent microtubule dynamics, Urol. Oncol. 32 (2014) 47 e21–48.

[49] D.M. Roy, L.A. Walsh, T.A. Chan, Driver mutations of cancer epigenomes, Protein Cell 5 (2014) 265–296.